

# Local structure effects of carbon-doping on the phase change material $\text{Ge}_2\text{Sb}_2\text{Te}_5$

John D. Langhout,<sup>†</sup> Danielle N. Alverson,<sup>†</sup> Colton Ginter,<sup>†</sup> Bruce Ravel,<sup>‡</sup>  
David Adams,<sup>¶</sup> and Megan M. Butala<sup>\*,†</sup>

<sup>†</sup>*Department of Materials Science and Engineering, University of Florida, Gainesville, FL  
32611*

<sup>‡</sup>*Material Measurement Laboratory, National Institute of Standards and Technology,  
Gaithersburg, MD 20899, USA, ORCID: 0000-0002-4126-872X*

<sup>¶</sup>*Sandia National Laboratories, Albuquerque, New Mexico 87185 USA*

E-mail: [mbutala@ufl.edu](mailto:mbutala@ufl.edu)

# Supporting Information

## 0.1 Additional XANES Information

XANES waterfall plots for GST-2% and GST-4% (Fig. S1) indicate crystallization between 140 °C and 150 °C. Unlike GST and GST-6%, this structure change occurs entirely between 140 °C and 150 °C; thus, the spectrum at 140 °C is fully amorphous and the spectrum at 150 °C is fully crystalline. Data collection for GST-2% is truncated at 220 °C because the thin film sample fell from the sample holder during in situ analysis.

In addition to the change in XANES spectra associated with crystallization, a decrease in the weighting of the crystalline phase above 200 °C is evident in GST, GST-4%, and GST-6%. This may be due to the emergence of a third phase, the trigonal phase, at elevated temperatures.<sup>1</sup> This phase features a similar local Ge environment to that of the rocksalt phase, which would cause slight differences in XANES spectra. While minor changes in XANES spectra, such as a decrease in white line intensity, are certainly reflected in the linear combination fitting results, we note that the trigonal phase is only reported to form between 200 °C and 300 °C at lower C concentrations.<sup>1</sup> However, we see here the onset of this phase in all compositions (except GST-2%, for which the data is truncated at 220 °C, and GST-12%, which never crystallized) irrespective of C-content. As a result, without accompanying diffraction or EXAFS structural fits, we cannot conclude with certainty that this behavior can be attributed to the formation of the trigonal phase.

The first derivative  $\frac{d\mu}{dE}$  of the normalized XANES for the lowest appropriate temperature of each composition are shown in Fig. S3. Edge energies were chosen by selecting the first inflection point of  $\mu(E)$ , i.e., the first maximum of  $\frac{d\mu}{dE}$ . The edge energies of GST, GST-2%, GST-4%, and GST-6% were nearly identical, although a slight shift to lower energy with carbon content is observed. GST-12% underwent a more significant energy shift, an increase of  $\approx 1.5$  eV. It must be noted that since all XAS data were taken in fluorescence mode as a result of their thick substrates, edge energies were not calibrated to a reference

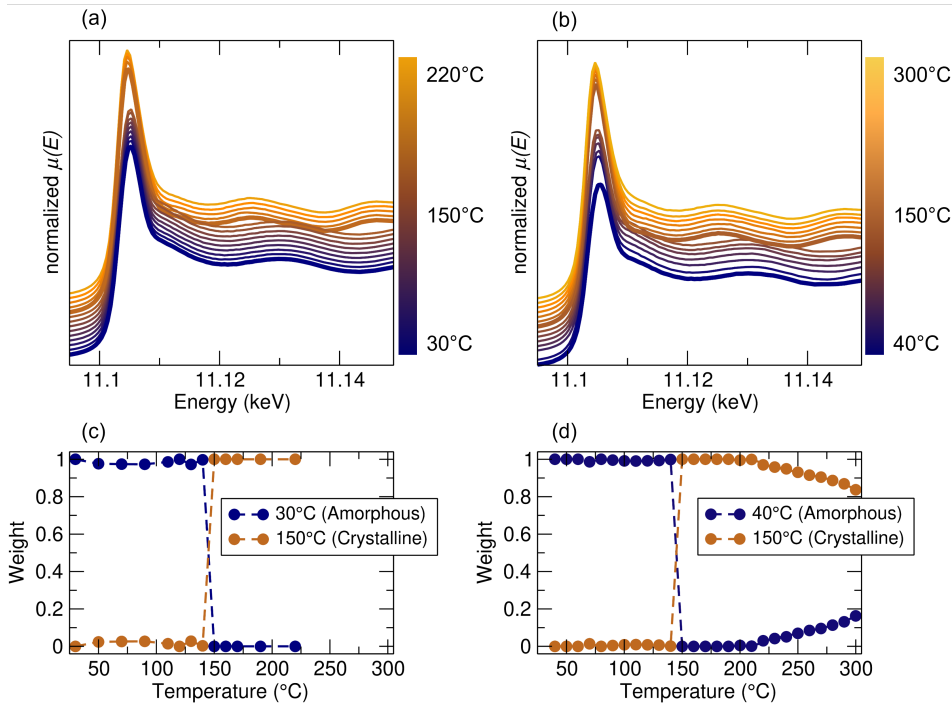


Figure S1: *In situ* XANES spectra for (a) GST-2% and (b) GST-4% show changes in the white line intensity and post-edge features during heating. Representative ‘amorphous’ and ‘crystalline’ spectra for each composition were used as models for linear combination fitting of (c) GST-2% and (d) GST-4% spectra, demonstrating the abrupt crystallization behavior. The reduced chi-square is below  $5 \times 10^{-3}$  for both shown fits.

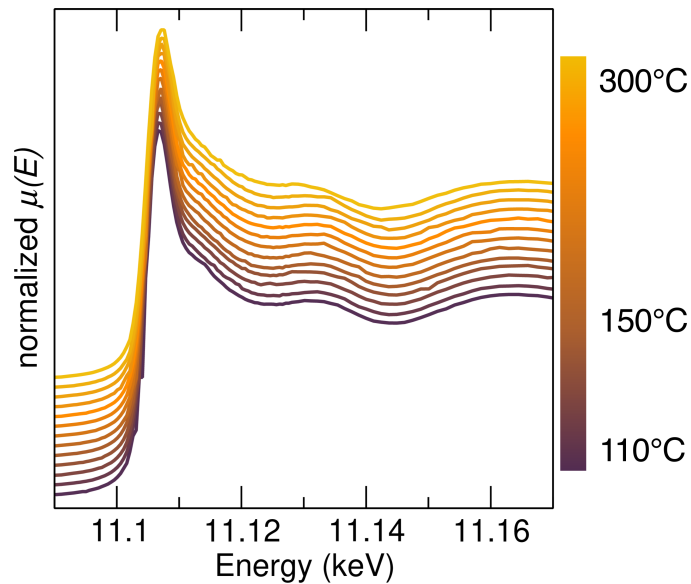


Figure S2: *In situ* XANES spectra for GST-12%.

Ge foil. However, only a change as high as  $\pm 0.5$  eV can realistically be attributed to an instrument energy drift, so we maintain that the increase in edge energy in GST-12% is physical.

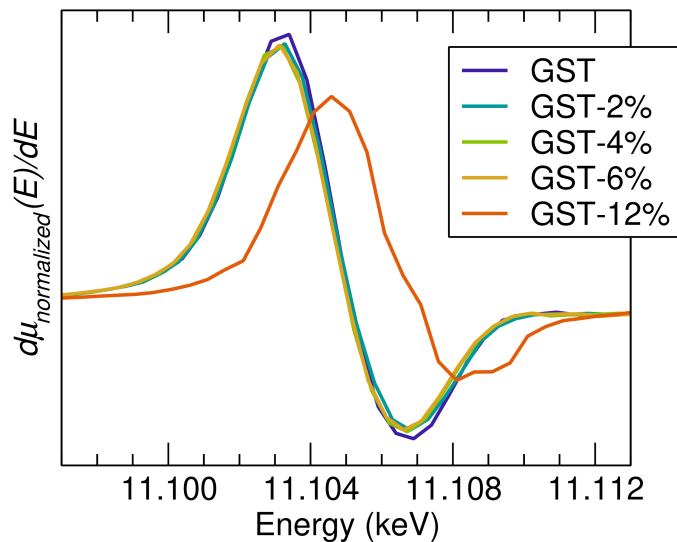


Figure S3:  $\frac{d\mu}{dE}$  for the lowest temperature (30 °C for GST, GST-4%, and GST-6%, 40 °C for GST-2%, and 110 °C for GST-12%) normalized XAFS spectrum of each composition.

## 0.2 Additional EXAFS Information

Comparing Fourier transformed EXAFS spectra of each composition (at the lowest measured temperature: 30 °C for GST, GST-4%, and GST-6%, 40 °C for GST-2%, and 110 °C for GST-12%) reveals the structural effect of carbon content. Note the feature centered at 1.4 Å that emerges in the doped samples and is the most intense in GST-12%. This is associated with a Ge–C path corresponding to a Ge–C bond  $\approx 1.85$  Å long. While this path is qualitatively visible in  $|\chi(R)|$ , the combination of the short path length, low scattering factor of C, and low concentration of C makes it prone to distortion during data reduction, particularly during background removal.<sup>2</sup> As a result, this path was not included in the reported structural models.

The Fourier transformed EXAFS spectrum of amorphous GST is consistent with an amorphous material. It contains a single strong feature which is modeled well using a

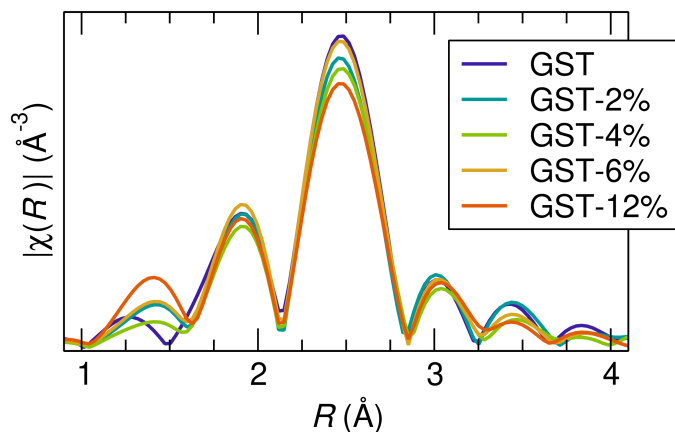


Figure S4: EXAFS spectra in  $|\chi(R)|$  for the lowest temperature (30 °C for GST, GST-4%, and GST-6%, 40 °C for GST-2%, and 110 °C for GST-12%) of all compositions.

single coordination shell. In comparison, the spectrum at 150 °C changes drastically. The first feature is pushed to higher  $R$  and broadens, likely as a result of an increase in Ge coordination from  $\approx 4$  to 6. Additionally, several features arise past this first feature, such as at 3.5 Å and 4.25 Å (Fig. S5). This is consistent with a more crystalline solid which displays additional coordination shells past the first.

Crystalline spectra were not fit due to poor data quality and the elevated temperatures, in which the length-dependency of  $\sigma^2$ ,<sup>3,4</sup> severely dampens the intensity of longer paths. Cubic rocksalt and trigonal atomic models were fit to crystalline EXAFS spectra, however, these fits were not presentable or physically meaningful enough to draw any conclusions appropriate for publication.

### 0.3 Additional EXAFS Fitting Information

The following spectra were omitted from analysis: GST-2% at 120 °C, GST-4% at 30 °C, and GST-4% at 80 °C. For the omitted GST-2% spectrum, unusually high levels of noise and significant artifacts created nonphysical features in  $|\chi(R)|$  that disrupted trends in  $R$ -factor and model fitting. For the omitted GST-4% XAFS spectra, XAS data were unexpectedly truncated at high  $E$ , decreasing the  $k$ -range, and thus the resolution of the Fourier-transformed spectra. Likewise, this incongruity in data quality made visualizing

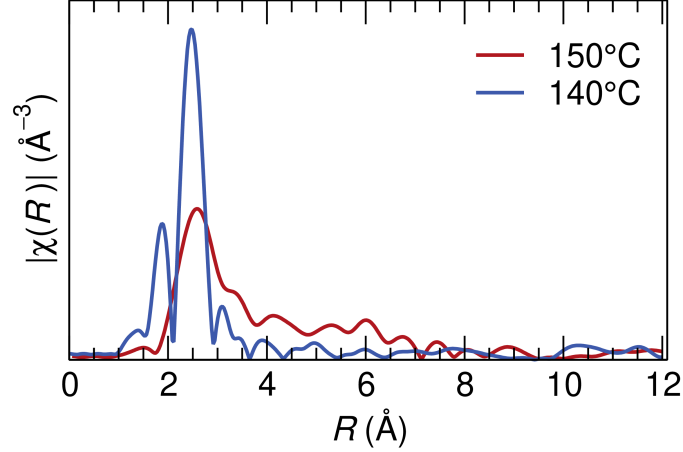


Figure S5: EXAFS spectra of GST at 140 °C (mostly amorphous) and 150 °C (crystalline).

data trends more difficult and thus, the data were omitted from figures.

EXAFS fitting series in which  $N_{Ge-Te}$  and  $N_{Ge-Ge}$  were the constrained variables (instead of  $\sigma_{Ge-Te}^2$  and  $\sigma_{Ge-Ge}^2$ ) were attempted. A roughly linear increase in  $\sigma_{Ge-Te}^2$  and  $\sigma_{Ge-Ge}^2$  with temperature was observed. However, the values of  $\sigma^2$  did not increase steadily and linearly, and the values retained a high level of uncertainty. We attribute this to a high correlation between  $\sigma_{Ge-Te}^2$  and  $\sigma_{Ge-Ge}^2$ . In contrast, constraining  $\sigma_{Ge-Te}^2$  and  $\sigma_{Ge-Ge}^2$ , as reported in the main section, led to a weaker correlation between  $N_{Ge-Te}$  and  $N_{Ge-Ge}$ , and thus to the steadier temperature-dependent behavior of the parameters.

Uncertainties in EXAFS fitting parameters (error bars in figures and  $\pm$  values in tables) are automatically calculated in LARCH, which utilizes the UNCERTAINTIES python package to generate standard error values.<sup>5</sup> The error bars denoted in  $N \cdot \sigma^2$  versus temperature plots are normalized to the value of  $\sigma^2$  as follows:  $Standard\ Error_{N \cdot \sigma^2} = \frac{Standard\ Error_N}{N} \cdot (N \cdot \sigma^2)$ . Note that since  $\sigma^2$  is held constant, only  $N$  has an associated standard error value.

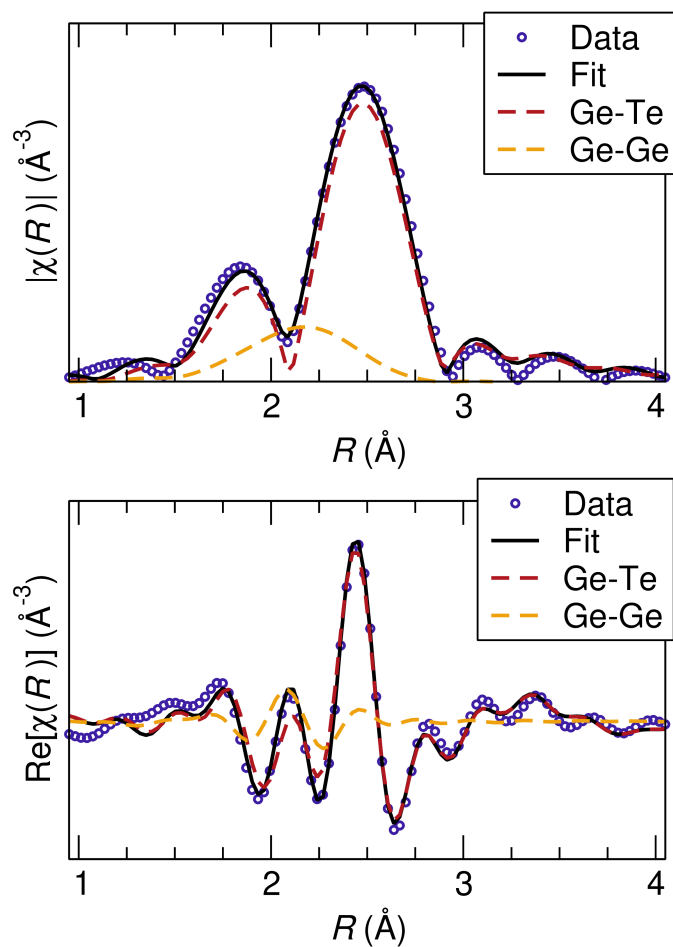


Figure S6: An example of an EXAFS fit of GST at 30 °C using a free model. The signal contributions in  $|\chi(R)|$  and  $Re[\chi(R)]$  of the Ge–Te and Ge–Ge paths are shown in red and yellow, respectively.

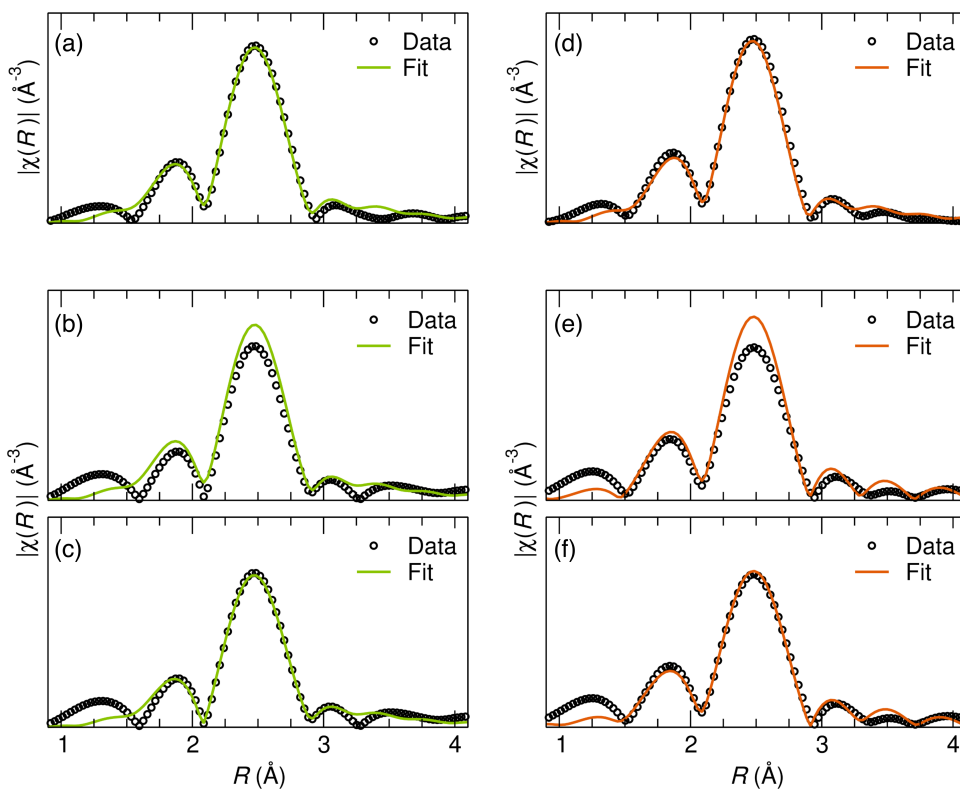


Figure S7: Additional EXAFS fits. Room temperature fits to room temperature spectra for (a) GST-4% and (d) GST-6%, room temperature models placed over high temperature amorphous spectra for (b) GST-4% and (e) GST-6%, and resulting fits of high temperature spectra following the constrained fitting method for (c) GST-4% and (f) GST-6%.

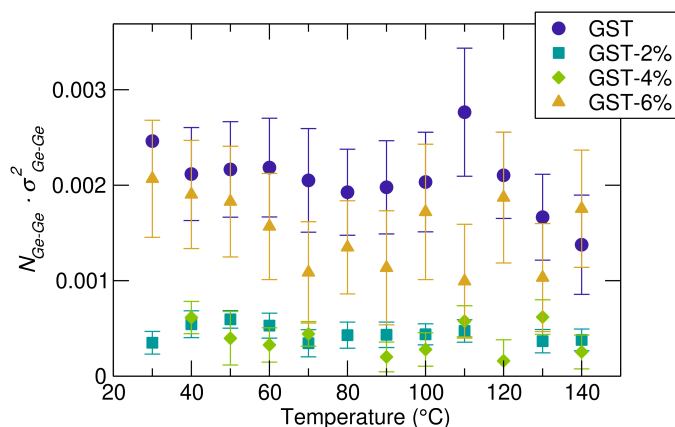


Figure S8: Results of the constrained fitting method, showing  $N_{Ge-Ge} \cdot \sigma_{Ge-Ge}^2$  versus temperature for each composition. The large error bars demonstrate the uncertainty regarding the Ge–Ge path in this study.

Table S1: EXAFS fitting results for lowest temperature spectrum of each composition. Uncertainties of fitting parameters are automatically calculated using LARCH, which employs the UNCERTAINTIES package to determine standard error.<sup>5</sup>

GST						
Temperature = 30 °C						
$R$ -factor = 0.0081						
$S_0^2 = 0.75$						
Bond	$N$	$\pm$	$r$ (Å)	$\pm$ (Å)	$\sigma^2$ (Å <sup>2</sup> )	$\pm$ (Å <sup>2</sup> )
Ge–Ge	0.48	0.64	2.464	0.0339	0.0023	0.6249
Ge–Te	3.09	0.25	2.6227	0.0129	0.0050	0.0015
GST-2%						
Temperature = 30 °C						
$R$ -factor = 0.0047						
$S_0^2 = 0.75$						
Bond	$N$	$\pm$	$r$ (Å)	$\pm$ (Å)	$\sigma^2$ (Å <sup>2</sup> )	$\pm$ (Å <sup>2</sup> )
Ge–Ge	0.16	0.59	2.4874	0.1055	0.0028	0.0337
Ge–Te	2.87	0.20	2.6185	0.0086	0.0046	0.0014
GST-4%						
Temperature = 40 °C						
$R$ -factor = 0.0183						
$S_0^2 = 0.75$						
Bond	$N$	$\pm$	$r$ (Å)	$\pm$ (Å)	$\sigma^2$ (Å <sup>2</sup> )	$\pm$ (Å <sup>2</sup> )
Ge–Ge	0.43	0.86	2.4750	0.0528	0.0021	0.2139
Ge–Te	3.19	0.40	2.6292	0.0195	0.0057	0.0021
GST-6%						
Temperature = 30 °C						
$R$ -factor = 0.0079						
$S_0^2 = 0.75$						
Bond	$N$	$\pm$	$r$ (Å)	$\pm$ (Å)	$\sigma^2$ (Å <sup>2</sup> )	$\pm$ (Å <sup>2</sup> )
Ge–Ge	0.26	1.05	2.4820	0.1128	0.0020	0.0055
Ge–Te	2.90	0.26	2.6182	0.0115	0.0039	0.0028
GST-12%						
Temperature = 110 °C						
$R$ -factor = 0.0243						
$S_0^2 = 0.75$						
Bond	$N$	$\pm$	$r$ (Å)	$\pm$ (Å)	$\sigma^2$ (Å <sup>2</sup> )	$\pm$ (Å <sup>2</sup> )
Ge–Ge	0.93	5.48	2.4885	0.0806	0.0100	0.0300
Ge–Te	3.10	0.48	2.6175	0.0101	0.0062	0.0018

Table S2: Linear regressions of  $N_{Ge-Te} \cdot \sigma_{Ge-Te}^2$  and  $N_{Ge-Ge} \cdot \sigma_{Ge-Ge}^2$  versus temperature.

Composition	Ge-Te		Ge-Ge	
	Slope ( $\times 10^{-5}$ )	$R^2$	Slope ( $\times 10^{-6}$ )	$R^2$
GST	-1.39	0.54	-3.4	0.41
GST-2%	-1.12	0.79	-0.9	0.15
GST-4%	-1.13	0.51	-1.2	0.55
GST-6%	-1.64	0.85	-4.25	0.16

## References

- (1) Scott, E. A.; Ziade, E.; Saltonstall, C. B.; McDonald, A. E.; Rodriguez, M. A.; Hopkins, P. E.; Beechem, T. E.; Adams, D. P. Thermal conductivity of  $(\text{Ge}_2\text{Sb}_2\text{Te}_5)_{1-x}\text{C}_x$  phase change films. *J. Appl. Phys.* **2020**, *128*, 155106.
- (2) Washington, J. S. P. The local structure and kinetics of germanium-antimony-tellurium phase change materials for use in solid state applications. Ph.D. thesis, 2010; Copyright - Database copyright ProQuest LLC; ProQuest does not claim copyright in the individual underlying works; Last updated - 2023-03-03.
- (3) Calvin, S. *XAFS For Everyone*; CRC Press: Boca Raton, 2013.
- (4) Ravel, B.; Kelly, S. D. The Difficult Chore of Measuring Coordination by EXAFS. *AIP Conf. Proc.* **2007**, *882*, 150–152.
- (5) Newville, M. Larch: An Analysis Package For XAFS And Related Spectroscopies. *J. Phys. Conf. Ser.* **2013**, *430*.